Interferometric tomography of fuel cells for monitoring membrane water content

Citation: Waller, Laura, Jungik Kim, Yang Shao-Horn, and George Barbastathis. Interferometric Tomography of Fuel Cells for Monitoring Membrane Water Content. Optics Express 17, no. 17 (August 6, 2009): 14806. © 2009 OSA

As Published: http://dx.doi.org/10.1364/OE.17.014806

Publisher: Optical Society of America

Persistent URL: http://hdl.handle.net/1721.1/79689

Version: Final published version: final published article, as it appeared in a journal, conference proceedings, or other formally published context

Interferometric tomography of fuel cells for monitoring membrane water content

Laura Waller,[1,*] Jungik Kim,[2] Yang Shao-Horn[2,3] and George Barbastathis[2,4]

[1]*Department of Electrical Engineering and Computer Science, Massachusetts Institute of Technology, 77 Massachusetts Avenue, Cambridge, MA 02139, USA*
[2]*Department of Mechanical Engineering, Massachusetts Institute of Technology, 77 Massachusetts Avenue, Cambridge, MA 02139, USA*
[3]*Department of Materials Science and Engineering, Massachusetts Institute of Technology, 77 Massachusetts Avenue, Cambridge, MA 02139, USA*
[4]*Singapore-MIT Alliance for Research and Technology (SMART) Center, 3 Science Drive 2, Singapore 117543*
**lwaller@mit.edu*

Abstract: We have developed a system that uses two 1D interferometric phase projections for reconstruction of 2D water content changes over time in situ in a proton exchange membrane (PEM) fuel cell system. By modifying the filtered backprojection tomographic algorithm, we are able to incorporate a priori information about the object distribution into a fast reconstruction algorithm which is suitable for real-time monitoring.

OCIS codes: (110.6960) Tomography; (120.3180) Interferometry.

References and links

1. A. LaConti, M. Hamilton, and R. McDonald, *Handbook of Fuel Cells – Fundamentals, Technology and Applications* (Wiley 2003).
2. D. Wilkinson, and J. St-Pierre, "In-plane gradients in fuel cell structure and conditions for higher performance," J. Power Sources **113**(1), 101–108 (2003).
3. S. Knights, K. Colbow, J. St-Pierre, and D. Wilkinson, "Aging mechanisms and lifetime of PEFC and DMFC," J. Power Sources **127**(1-2), 127–134 (2004).
4. U. Pasaogullari, and C. Wang, "Liquid water transport in gas diffusion layer of polymer electrolyte fuel cells," J. Electrochem. Soc. **151**(3), A399–A406 (2004).
5. J. St-Pierre, "PEMFC in situ liquid water content monitoring status," J. Electrochem. Soc. **154**(7), B724–B731 (2007).
6. S. Tsushima, K. Teranishi, K. Nishida, and S. Hirai, "Water content distribution in a polymer electrolyte membrane for advanced fuel cell system with liquid water supply," Magn. Reson. Imaging **23**(2), 255–258 (2005).
7. R. Satija, D. Jacobson, M. Arif, and S. Werner, "In situ neutron imaging technique for evaluation of water management systems in operating PEM fuel cells," J. Power Sources **129**(2), 238–245 (2004).
8. Y. Patil, T. Seery, M. Shaw, and R. Parnas, "In situ water sensing in a Nafion membrane by fluorescence spectroscopy," Ind. Eng. Chem. Res. **44**(16), 6141–6147 (2005).
9. E. Alanis, G. Romero, and C. Martinez, "Interferometric measurement of diffusion coefficients through a scanning laser beam," Opt. Eng. **39**(3), 744–750 (2000).
10. J. Kim, L. Waller, G. Barbastathis, and Y. Shao-Horn, "Temperature and water content measurements of Nafion membrane in PEM fuel cells by laser interferometry," in *Proceedings of Electrochem. Soc.,* (2005).
11. J. Kim, L. Waller, G. Barbastathis, and Y. Shao-Horn, "Methodology to understand the degradation mechanism of Nafion membrane in PEM fuel cells," in *Electrochem. Soc. Trans.* 1(8), 323–334 (2006).
12. J. Kim, L. Waller, G. Barbastathis, and Y. Shao-Horn, "Water transport in Nafion membrane measured by laser interferometry," in *Proceedings of Electrochem. Soc.,* 702(420), (2007).
13. A. P. Leis, S. Schlicher, H. Franke, and M. Strathmann, "Optically transparent porous medium for nondestructive studies of microbial biofilm architecture and transport dynamics," Appl. Environ. Microbiol. **71**(8), 4801–4808 (2005).
14. J. Kong, *Electromagnetic Wave Theory* (EMW Publishing, 2000).
15. J. Fienup, "Phase retrieval algorithms: a comparison," Appl. Opt. **21**(15), 2758–2769 (1982).
16. M. Weiss, R. Srivastava, and H. Groger, "Experimental investigation of a surface Plasmon-based integrated-optic humidity sensor," Electron. Lett. **32**(9), 842–843 (1996).
17. P. Choi, and R. Datta, "Sorption in Proton-exchange membranes," J. Electrochem. Soc. **150**(12), E601–E607 (2003).
18. D. Ghiglia, and M. Pritt, *Two-dimensional Phase Unwrapping – Theory, Algorithms and Software* (Wiley Blackwell, 1998).

#111498 - $15.00 USD Received 18 May 2009; revised 24 Jul 2009; accepted 26 Jul 2009; published 6 Aug 2009

19. J. Huntley, and H. Saldner, "Temporal phase-unwrapping algorithm for automated interferogram analysis," Appl. Opt. **32**(17), 3047–3051 (1993).
20. A. Kak, and M. Slaney, *Principals of Computerized Tomographic Imaging* (Soc. Ind. Appl. Math., 2001).
21. M. Bertero, *Inverse Problems in Imaging* (Inst. Of Physics, 2002).
22. T. Olsen, "Stabalized inversion for limited angle tomography," Wavelet Applications **II**, 781–793 (1995).
23. A. F. Abouraddy, O. Shapira, M. Bayindir, J. Arnold, F. Sorin, D. S. Hinczewski, J. D. Joannopoulos, and Y. Fink, "Large-scale optical-field measurements with geometric fibre constructs," Nat. Mater. **5**(7), 532–536 (2006).
24. R. Rangayyan, A. P. Dhawan, and R. Gordon, "Algorithms for limited-view computed tomography: an annotated bibliography and a challenge," Appl. Opt. **24**(23), 4000–4013 (1985).
25. T. Inouye, "Image reconstruction with limited angle projection data," Trans. Nuclear Sci. **26**, 2666–2671 (1979).
26. M. Davison, "The ill-conditioned nature of the limited angle tomography problem," SIAM J. Appl. Math. **43**(2), 428–448 (1983).
27. E. Payot, F. Preteux, Y. Trousset, and R. Guillemaud, "3D reconstruction from incomplete Fourier spectra: An extrapolation approach," Statistical and Stochastic Methods for Image Proc. **2823**, 160–173 (1996).
28. K. Tam, and V. Perez-Mendez, "Tomographical imaging with limited-angle input," J. Opt. Soc. Am. **71**(5), 582–593 (1981).
29. M. Ravichandran, and F. Gouldin, "Reconstruction of smooth distributions from a limited number of projections," Appl. Opt. **27**(19), 4084–4097 (1988).
30. A. Oppenheim, R. Schafer, and J. Buck, *Discrete-time Signal Processing* (Prentice Hall, 1999)
31. S. Motupally, A. Becker, and J. Weidner, "Diffusion of water in Nafion 115 membranes," J. Electrochem. Soc. **147**(9), 3171–3177 (2000).
32. T. Zawodzinski, T. Springer, J. Davey, R. Jestel, C. Lopez, J. Valerio, and J. Gottesfeld, "A comparative study of water uptake by and transport through ionomeric fuel cell membranes," J. Electrochem. Soc. **140**(7), 1981–1985 (1993).

1. Introduction

Fuel cells are compact, reliable sources of clean energy. A PEM fuel cell consists of current collectors, an anode and a cathode, separated by a thin membrane. Hydrogen gas and oxygen are supplied to the anode and cathode sides, respectively, through gas flow channels, as shown in Fig. 1. Hydrogen molecules are oxidized at the anode to protons, which pass through the membrane, and electrons, which go through the circuit and flow to the cathode. On the other side, protons and electrons combine with supplied oxygen to form water.

The performance and failure of PEM fuel cell systems is critically dependent on the local water content in the membrane [1]. High humidity increases the fuel cell efficiency and also prevents degradation [2,3]. However, excessive humidity causes condensed droplets to form in the flow channels, locally blocking the reaction [4]. In order to design more durable and efficient systems, it is desired to detect water content changes while the fuel cell is in operation [5]. Furthermore, real-time monitoring of the local water content could be used as input to a feedback control system which would maintain ideal humidity across the entire membrane during operation.

Several groups have developed methods of imaging water content in fuel cell systems, using Magnetic Resonance Imaging [6], Neutron imaging [7], and optical fluorescence spectroscopy [8]. However, all of these methods are either invasive, expensive or have poor spatial or temporal resolution. St-Pierre [5] reviews and compares many of the different methods and explains their advantages and disadvantages. The end goal is to develop a real-time water imaging method which is inexpensive, non-invasive, and has both good spatial resolution and good temporal resolution.

We present here a system using interferometric phase tomography for 2D in situ monitoring of the water content in the membrane, with high spatial and temporal resolution, from 1D projection data. We assume that the refractive index is directly proportional to water content, and we measure the membrane to be better than 95% optically clear. Interferometry has proved useful for concentration gradient measurements of transparent liquid solutions [9], and we have shown previously that it is also suitable for measuring water concentration gradients in solid Nafion® membranes [10,11]. In these experiments, light was shone through the flat face of the membrane; thus, water content changes cause small changes in optical path length (OPL). For in situ measurements, light cannot be shone through the face of the membrane, as the surrounding electrodes are opaque (see Fig. 1). Thus, we shine the light through the length of the membrane, 'in-plane'. Preliminary results from this in-plane

#111498 - $15.00 USD Received 18 May 2009; revised 24 Jul 2009; accepted 26 Jul 2009; published 6 Aug 2009

configuration were demonstrated in [12]. Nafion®'s refractive index is very close to that of water, and it is sometimes used for index-matching in biofilms [13]. This means that the index changes due to humidity are very small (~10^{-4}/%RH); however, in the in-plane configuration, the OPL is longer by orders of magnitude than in the through-plane case, causing serious problems with aliasing in the phase unwrapping process, as well as increased internal absorption and refraction. Here, we show how these problems can be avoided by unwrapping the phase temporally instead of spatially, as well as optimizing the system for maximal contrast. Further, we require a 2D reconstruction of the water content (phase), so we add here a second angle of phase projection data, then reconstruct the 2D water content distribution tomographically, using a modified filtered-backprojection algorithm. This presents a new and interesting problem caused by the physical limitation on number of projection angles, namely, the reconstruction of tomography data from a severely limited number of reconstructions. Generally, two angles will not be enough to recover accurately a 2D distribution. However, by taking advantage of the inherently smooth and well-known diffusion process of the water in time and space, we are able to modify the backprojection filter with this a priori information in such a way as to reduce the error in the 2D reconstruction.

We show here theoretically and experimentally that our system is able to successfully detect and localize large changes in water content, such as those caused by condensation of a droplet of water in the flow channel. The optical system is described in Section 2. Signal processing considerations, relating to temporal vs spatial sampling requirements for phase unwrapping, and sparse angle tomography are presented in Section 3. Results are shown in Section 4, and conclusions are in Section 5.

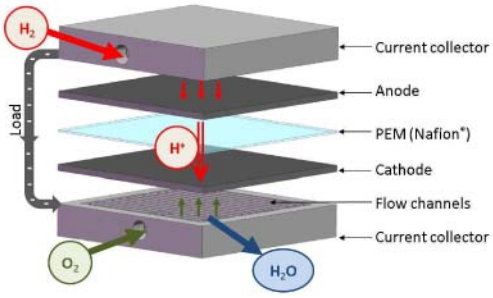

Fig. 1. PEM fuel cell system schematic.

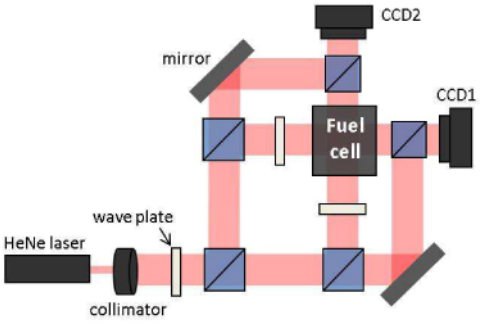

Fig. 2. Double Mach-Zehnder interferometer.

2. Optical system

The PEM fuel cell system sandwiches a 3cm x 3cm x 125µm semi-transparent membrane between two 7cm x 7cm x 2cm opaque current collectors with flow channels etched into them (see Fig. 1). Light is shone in-plane from two orthogonal angles using the custom designed

#111498 - $15.00 USD Received 18 May 2009; revised 24 Jul 2009; accepted 26 Jul 2009; published 6 Aug 2009

double Mach-Zehnder interferometer shown in Fig. 2. We model the fuel cell as a thick slit with a complex transmission function, due to line integrals of absorption and refractive index through the membrane. For each angle, we record the interference between the diffracted field from the slit and a plane wave reference (Fig. 3). Figure 4(a) shows a sample interferogram. We then reconstruct via our modified inverse Radon transform, as described in Section 3. The specific attributes of our system provide some unique considerations and challenges.

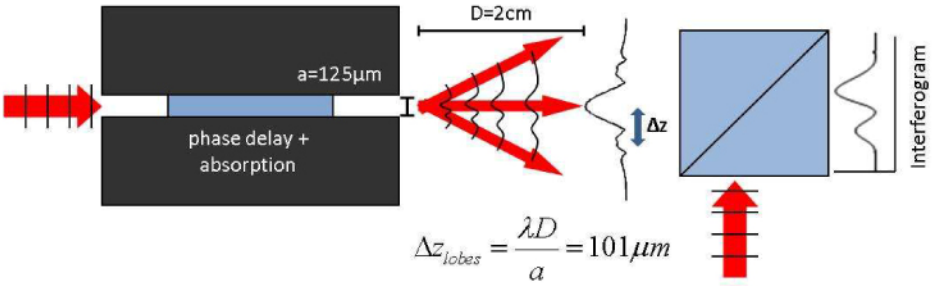

Fig. 3. Optical model of light through the system.

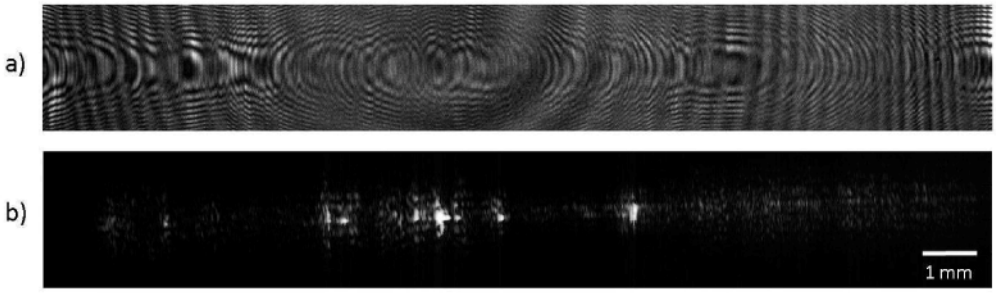

Fig. 4. In-plane images. (a) Interferogram at one camera. (b) Amplitude only.

First, the relatively long object OPL (3cm, n~1.33) means that there is more absorption than in the through-plane case. As can be seen in Fig. 4(b), inhomogeneity in the membrane causes intensity variation at the camera due to uneven absorption (and scatter). Since we interfere this beam with a plane wave of constant intensity, the parts of the object beam whose intensity matches that of the reference beam will have higher contrast. To get maximum overall contrast at our interferogram, we use a polarized beam splitter and three half wave plates to adjust the relative intensities of the beams such that the reference beam intensity matches that of the median object beam intensity, which is measured independently.

In order to assume straight rays through the membrane, internal refraction, which is dependent upon the refractive index gradient across the membrane, must not cause large bending of the rays through the membrane. In a worst-case scenario, when the center of the membrane is wet while the outer edges remain dry, we calculate a maximum ray deflection angle of 0.062rad. Thus, to avoid large errors due to internal refraction, the camera should be placed well within the 0.8m focal length. Since our experiment uses a camera distance of 54mm from the slit, we may confidently ignore internal refraction effects.

The external scatter that occurs at the input and output edges of the membrane is, however, a prominent effect. The face of the membrane is optically smooth, whereas the 125µm edges are cut with a blade, leaving striations and micron-scale jagged edges that scatter the light (see Fig. 5(a-b)). In this experiment, the rough edges were polished with 12,000 grit sandpaper until they were optically smooth. The reduction in roughness and edge scatter can be seen in Fig. 5(c-d). This polishing step greatly improves the contrast of the interferograms, and therefore the phase detection sensitivity. Furthermore, the diminished scatter from the edges reduces information crosstalk in the lateral direction, improving spatial resolution.

#111498 - $15.00 USD Received 18 May 2009; revised 24 Jul 2009; accepted 26 Jul 2009; published 6 Aug 2009

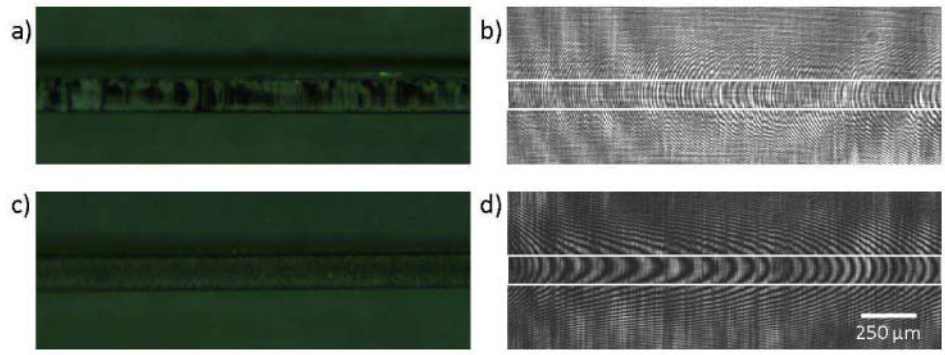

Fig. 5. The effect of polishing membrane edges. (a) Unpolished membrane edge, (b) interferogram of unpolished membrane edge, (c) polished membrane edge, (d) interferogram of polished membrane edge.

Waveguiding effects within the membrane may also be ignored. At $\lambda = 632.8$ nm, 347 TE modes are above cut-off, according to waveguide theory [14]. However, the sandwiching black electrodes, which are much larger than the membrane itself, are highly absorptive. Higher order modes are attenuated, even before they enter the membrane, and only the zero-order mode will pass through the system. The angular selectivity for the entire system is 1.8mrad when the system is properly aligned.

Diffraction in the vertical direction from the slit created by the fuel cell electrodes will cause reduced signal intensity at the 1D line of interest in the interferogram. The effect is predictable and reversible when a 2D camera image is available, using numerical backpropagation techniques. Digital holography alone, without phase-shifting, cannot accurately recover both amplitude and phase at the slit. Thus, we explored the use of iterative nonlinear optimization via Gerchberg-Saxton-Fienup algorithms in the Fresnel domain [15] (see Fig. 6). In this case, strong support constraints imposed by the opaque electrodes significantly reduces the solution space; however, uniqueness is not guaranteed. More importantly, these techniques are highly computational and not currently suitable for real-time implementation. In our case, we have shown that a straight ray assumption is valid, so we can significantly save computation and reduce data storage for high frame rates by collecting only the 1D line of interest and processing the data as described in Section 3.

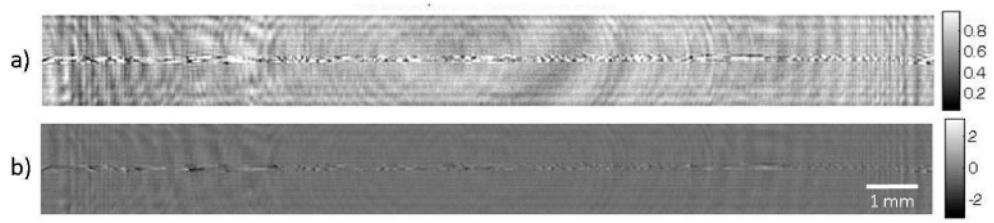

Fig. 6. Backpropagated solution using Gerchberg-Saxton-Fienup type iterative method in the Fresnel domain, after 50 iterations. (a) Amplitude and (b) Phase.

3. Sampling and Processing of data

3.1 Sampling diffusion-driven distributions

The interferometer intensity at the detector plane for a projection across y, neglecting diffraction and refraction, is given as follows:

$$I(x,t) = I_r + I_o(x,t) + 2\sqrt{I_r I_o(x,t)}\cos\left(\frac{2\pi}{\lambda}\int_Y \Delta n(x,y,t)dy\right)$$

#111498 - $15.00 USD Received 18 May 2009; revised 24 Jul 2009; accepted 26 Jul 2009; published 6 Aug 2009

where I_r is the reference beam intensity (assumed to be uniform), $I_o(x,t)$ is the object beam intensity, $\lambda = 632.8$ nm is the HeNe laser wavelength, Y is the membrane length in the y direction, and $\Delta n(x,y,t) = \frac{\partial n}{\partial \Lambda}\Delta\Lambda(x,y,t)$ is the refractive index in the plane of the membrane, where Λ is the water content of the membrane. Water content is defined as the ratio of water molecules to Nafion® molecules, with $\Lambda_{dry} \approx 2$ and $\Lambda_{wet} \approx 20$. The expression for the projection across x, $I(y,t)$ is analogous. The measured phase $\phi_x(x,t)$ which wraps every 2π, is

$$\phi_x(x,t) = \frac{2\pi}{\lambda}\int_Y \frac{\partial n}{\partial \Lambda}\Delta\Lambda(x,y,t)dy.$$

After obtaining two data sets of projections over time, our reconstruction algorithm goes as follows. For each pixel along x, variations in water content over time appear as changes in frequency of intensity oscillations (Fig. 7(a)). Fast oscillations indicate large changes in water content. A simple peak and valley detection algorithm is applied to the intensity vs time data, then the phase is cumulatively integrated across time, adding π for each subsequent peak or valley. This unwrapped phase data is linearly interpolated and multiplied by the known constant, $\partial n / \partial \Lambda$, as measured in previous literature [16,17], to convert it to water content (Fig. 7(b)).

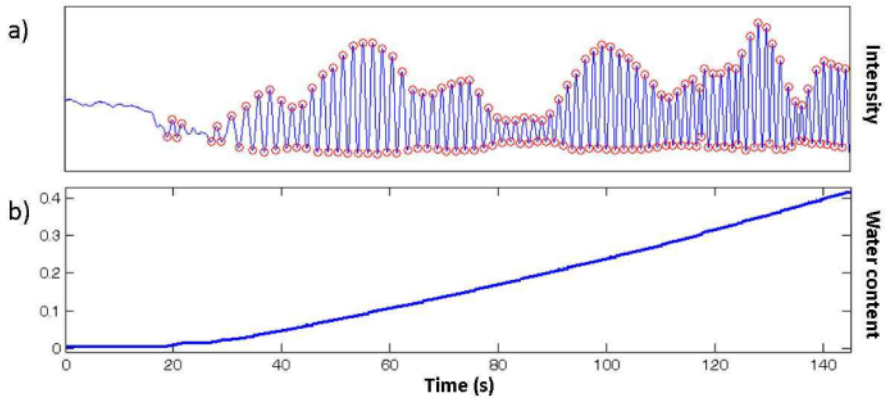

Fig. 7. Unwrapping intensity variations for one pixel. (a) Intensity vs time for one projection pixel, while humidifying. Circles indicate detected peaks and valleys for unwrapping, (b) Water content change vs time after phase unwrapping and conversion to water content changes.

Usually, phase unwrapping is done in the spatial domain. Algorithms attempt to integrate the measured cosine of the phase over the entire 1D or 2D domain. Any noise or phase discontinuity makes the inversion ill-posed and various algorithms have been developed to best approximate the true phase [18]. All of these methods, however, carry the restriction that the phase difference between two adjacent pixels must not exceed π, in order to avoid aliasing in the unwrapping process. This restriction is much more difficult to meet when using a long OPL, as in our case. To avoid wrapped phase aliasing in diffusion interferometry, we show below that it is better to use temporal, rather than spatial, unwrapping of the phase.

Given that water can only diffuse into and through the membrane, the water content distribution must be a solution to the diffusion equation,

$$\frac{\partial \Lambda}{\partial t} = D\frac{\partial^2 \Lambda}{\partial x^2}.$$

Assuming a linear diffusion coefficient, D, the change in water content over x due to a step variation is

#111498 - $15.00 USD Received 18 May 2009; revised 24 Jul 2009; accepted 26 Jul 2009; published 6 Aug 2009

$$\frac{\partial \Lambda}{\partial x} = (\Lambda_f - \Lambda_i)\frac{\partial}{\partial x}\left[\operatorname{erfc}\left(\frac{x}{\sqrt{4Dt}}\right)\right],$$

where Λ_f and Λ_i are the final and initial water content in the membrane, respectively. Using this solution, we require that the phase difference between pixels be less than π to avoid aliasing, and substitute known values of our system to get the minimum spatial sampling:

$$\frac{1}{\Delta x_{\max}} = \left(\frac{\partial \Lambda}{\partial x_{\max}}\right)\left(\frac{\partial \phi}{\partial \Lambda}\right)\left(\frac{\text{sample}}{\pi}\right) = \frac{6\text{samples}}{\mu m}$$

If we attempted to measure such a fast phase change, we would be violating our own weak scattering assumption. On the other hand, the temporal derivative of water content in a diffusion profile is:

$$\frac{\partial \Lambda}{\partial t} = \left(\frac{\partial \Lambda}{\partial x}\right)\left(\frac{x}{2t}\right)$$

which leads to a minimum temporal sampling:

$$\frac{1}{\Delta t_{\max}} = \left(\frac{\partial \Lambda}{\partial t_{\max}}\right)\left(\frac{\partial \phi}{\partial \Lambda}\right)\left(\frac{\text{sample}}{\pi}\right) = \frac{352\text{samples}}{\text{sec}}$$

It is easy to find inexpensive cameras or line sensors achieving frame rates above 352fps. Thus, temporal unwrapping will give us valid reconstructions, where spatial unwrapping would not.

3.2 Temporal phase unwrapping

Temporal phase unwrapping was first proposed by Huntley and Saldner [19] in terms of fringe projection profiling. They took many interferograms while shifting the fringe pitch, then unwrapped each pixel independently of the others, in order to reconstruct a single 2D unwrapped phase image without reverting to complicated 2D phase unwrapping techniques, which are unstable, non-unique, and computationally expensive [18]. Another advantage of temporal phase unwrapping is that there are no restrictions on the spatial smoothness of the phase, since the unwrapping process occurs across time.

In our approach to temporal phase unwrapping, phase changes are not actively induced in the reference beam, as this would greatly reduce our effective frame rate. Rather, the phase changes are precisely what we are trying to measure from the object beam. Thus, we essentially perform a differential phase measurement. We assume an initial state of a dry and homogenous membrane, and measure the changes from the initial state over time. The intrinsic temporal smoothness of water diffusion curves aids in reducing error and relaxing the sampling restrictions.

Once the temporally unwrapped phase is computed for each projection set, yielding the data sets $\phi_x(x,t)$ and $\phi_y(y,t)$, the two projection sets are then used to tomographically reconstruct the phase at each time sample. A naive application of the inverse Radon transform will yield useless results due to the huge amount of missing information; thus, we must modify our reconstruction algorithm to suit the system, as described below.

3.3 Sparse angle tomography

Tomography introduces inherent error, due to finite data in the projection-slice theorem [20] and interpolation between projections. A general rule for managing interpolation error is that the number of samples in each projection, N, should be similar to the number of projections, N_{proj} [20]. Using a 1200 pixel camera would imply that we should measure the phase at 1200 evenly spaced projection angles. We show here that the inherent spatial and temporal smoothness of the water diffusion process, combined with a desire only for low resolution

#111498 - $15.00 USD Received 18 May 2009; revised 24 Jul 2009; accepted 26 Jul 2009; published 6 Aug 2009

information, allows us to drastically decrease the number of required projection angles, while still accurately detecting and localizing water content changes. The resolution of the reconstructed images could be improved by adding more projection angles to the system, at the expense of added complexity and reduced field of view.

The Fourier Slice Theorem states that the 1D Fourier transform of a projection specifies a line in the 2D Fourier transform of the object at the corresponding angle [21]. As more angles are added to the reconstruction, low frequencies near the origin become oversampled, while higher frequencies are more sparsely sampled. Missing high frequency data cannot be interpolated accurately without a priori information. However, low frequency data can still be accurately reconstructed with few projection angles [22]. In the extreme case of only two projection angles, where we collect 2N data points and try to reconstruct an N^2 image, we expect only the lower frequency data to be properly reconstructed. An example of two angle tomography in a different context is shown in [23].

Limited angle tomography has been extensively studied [24] due to its importance in medical imaging, where some projection angles may not be physically feasible. Most studies deal with limited angular range rather than sparse angular sampling [25]. The solution is generally nonunique and unstable [26], so a priori information is important for extrapolating the missing data [27]. Nonlinear iterative methods (maximum entropy) can easily incorporate a priori information [28]; however, they are slow and computationally expensive when compared to direct methods, and so do not lend themselves to real-time reconstructions. Here, we use a Fourier domain reconstruction method which is fast enough to be used in real-time.

In order to get reasonable reconstructions from the tomographic data, we use a custom designed backprojection filter. An overcomplete, redundant basis set with redundancy has been previously used for recovering low-resolution information [22]. Here, we choose the Kaiser backprojection filter, suggested as a basis for reconstructing smooth distributions [29]. In the case of only two projection angles, there is no need for a ramp interpolation filter, and we simply place the Fourier domain projections in the center row and column of the Fourier domain reconstruction, averaging the DC term,

$$\Phi(u \neq 0, 0, t) = \mathcal{F}\{\phi_x(x,t)\}K(u);$$

$$\Phi(0, v \neq 0, t) = \mathcal{F}\{\phi_y(y,t)\}K(v);$$

$$\Phi(0,0,t) = (\mathcal{F}\{\phi_y(0,t)\} + \mathcal{F}\{\phi_y(0,t)\})/2;$$

where Φ is the 2D Fourier transform of the phase reconstruction, with spatial frequency variables u and v, $\mathcal{F}$ denotes a 1D Fourier transform, and $K(u)$ is the Kaiser window in Fourier domain, defined as [30],

$$K(u) = \frac{I_0(\beta(C^2 - u^2)^{0.5})}{I_0(\beta)},$$

with I_0 being the modified Bessel function of the first kind, order 0, C the cutoff frequency for the window, and β controls the spatial influence of the basis functions. Our C parameter is set at the maximum frequency expected from diffusion of water into Nafion®, given that the water must diffuse through half the vertical thickness of the membrane before a measurement is taken. A fairly large β value of 5 was chosen to match the spreading of water from a point source, based on the diffusion coefficient. Indeed, the Gaussian function is a solution to the diffusion equation, and the Kaiser function with large β tends to a Gaussian curve in frequency and object spaces. While a Gaussian curve technically has infinite bandwidth, we assume that it is effectively bandlimited by the noise floor of the camera. Thus, for our experimental configuration, the expected effective bandwidth covers only the lower 6% of the available bandwidth determined by the spatial sampling of the camera. Happily, this low

#111498 - $15.00 USD Received 18 May 2009; revised 24 Jul 2009; accepted 26 Jul 2009; published 6 Aug 2009

frequency information is also the area in frequency space which has the least interpolation error. By redesigning the filter in the backprojection method to restrict the solutions to the class that we are looking for, we eliminate the higher frequency information that would normally corrupt the image. Thus, it is only with the a priori knowledge of the expected water content distribution smoothness that we are able to reconstruct an accurate image, despite the huge amount of missing information in this inverse problem. Here, we have used a Fourier Domain method to keep the reconstructions fast for real-time applications. The separability and isotropy of the basis functions could be further exploited for efficient display and storage of computed data.

4. Experimental results

A simple test object was built, consisting of two 15mm x 15mm aluminum plates sandwiching a Nafion® membrane of the same dimensions. The top aluminum plate has a 2mm radius hole drilled into it. A drop of water was placed in this hole, and the 1D interferogram data were collected and processed from both cameras. Frames from the 500fps 2D experimental reconstruction video are shown in Fig. 8 (Media 1), with an overlaid white circle indicating the hole position. As expected, water content originates within the hole then diffuses outward into the surrounding regions. The positional accuracy of the water drop centroid is less than 1mm throughout the experiment's duration. The reconstruction has visible T-shaped artifacts, due to the two orthogonal angles used. The artifacts make for poor visual quality in the reconstructions, but they do not impact the accuracy of localization of damage due to increased water uptake, which is our intended outcome from this experiment. If only large changes in water content need to be detected, such as those which occur when a water drop forms in the flow channel, then a simple threshold process may be applied to the reconstruction to detect only areas with large water content changes. Such a modification would be useful in real-time feedback control of the membrane humidity, where we do not require high resolution images, but rather simple detection and 2D position of changes.

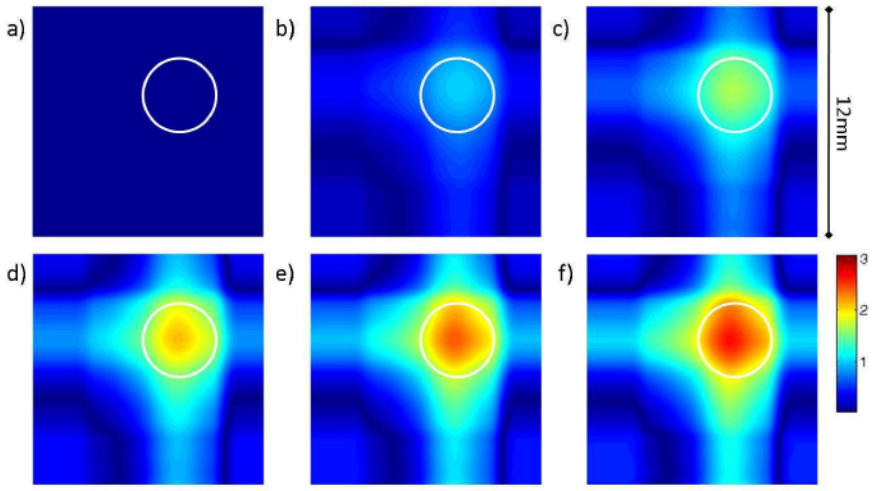

Fig. 8. Experimental reconstruction of water content in our test object after a) 0 s, b) 160 s, c) 320 s, d) 480 s, e) 640 s, f) 800 s. White circle indicates location of water drop (Media 1).

Next, the system was used to monitor water content in situ in a PEM fuel cell. For this experiment, the water was introduced by flowing humidified air through the flow channels. A finite element (FEM) simulation of the expected water content profile near one corner of the flow channel area, and its projections, are shown in Fig. 9(a). For this simulation, a nonlinear diffusion coefficient was used [31,32].

#111498 - $15.00 USD Received 18 May 2009; revised 24 Jul 2009; accepted 26 Jul 2009; published 6 Aug 2009

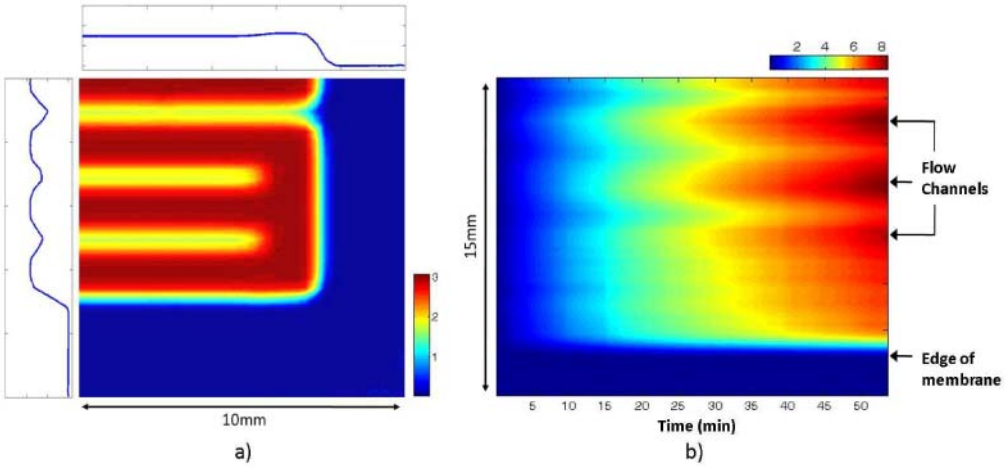

Fig. 9. (a) FEM simulation of water diffusing from flow channels into Nafion® membrane after 3 min. (b) Experimental water content projection data over time from one camera.

In the experimental data, when we look at a subsection of the data from one angle over time, we are able to resolve three individual flow channels taking on water over time faster than their surrounding areas on the membrane (see Fig. 9(b)). These experimental results show the overall water content in the membrane increasing greatly in the area where the flow channels are present, then diffusing to the outer areas via in-plane diffusion. As expected, no water content is detected outside the area of the membrane.

Figure 10 shows tomographically reconstructed frames of 2D water content distribution, recovered from the full two angle projection data. As expected, the water is introduced into the membrane first in the area where the flow channels are present, then diffuses outward to the rest of the membrane. The computed water content maximum values are consistently somewhat lower than expected, most likely due to the information spreading caused by few angle tomographic reconstruction.

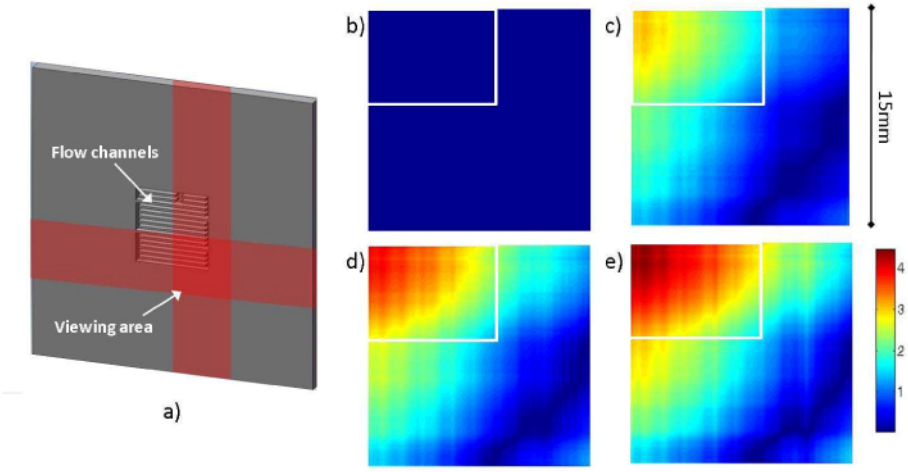

Fig. 10. Experimental water content reconstruction for a PEM fuel system. (a) Position of viewing area during experiment. 2D water content reconstructions after (b) 0 min (c) 15 min (c) 45 min (f) 95 min.

#111498 - $15.00 USD Received 18 May 2009; revised 24 Jul 2009; accepted 26 Jul 2009; published 6 Aug 2009

5. Conclusion

We have demonstrated a system capable of in situ monitoring of water content changes in a PEM fuel cell system by using two-angle interferometric phase tomography with temporal unwrapping of the phase data before conversion to water content data. The unique constraints of the system require modification of standard techniques for phase unwrapping and tomographic reconstruction. We are nevertheless able to obtain reasonable reconstructions of the water content in the fuel cell membrane with only two projection angles, by using a priori knowledge of the distribution smoothness in space and time. This system forms the possible basis for a real-time monitoring system that could be integrated with feedback to keep the fuel cell system operating at maximum efficiency and to prevent failure. Future work might include parallel analysis of a multi-cell fuel cell stack, and deconvolution techniques for postprocessing the phase reconstructions, which have a known point spread function.

Acknowledgements

We are grateful to the 3D Optical Systems group members for helpful discussions and assistance in the laboratory, and to the DuPont-MIT Alliance and the Singapore-MIT Alliance for Research and Technology (SMART) Centre for financial support.

#111498 - $15.00 USD Received 18 May 2009; revised 24 Jul 2009; accepted 26 Jul 2009; published 6 Aug 2009